

**2016 NDIA GROUND VEHICLE SYSTEMS ENGINEERING AND TECHNOLOGY
SYMPOSIUM
MODELING & SIMULATION, TESTING AND VALIDATION (MSTV) TECHNICAL SESSION
AUGUST 2-4, 2016 - NOVI, MICHIGAN**

**PREDICTION OF VEHICLE MOBILITY ON LARGE-SCALE SOFT-SOIL
TERRAIN MAPS USING PHYSICS-BASED SIMULATION**

Tamer M. Wasfy, PhD
Advanced Science and Automation Corp.
Indianapolis, IN

Paramsothy Jayakumar, PhD
U.S. Army TARDEC
Warren, MI

Dave Mechergui
U.S. Army TARDEC
Warren, MI

Srinivas Sanikommu
U.S. Army TARDEC
Warren, MI

ABSTRACT

*A high-fidelity physics-based approach for predicting vehicle mobility over large terrain maps is presented. The novelties of this paper are: (i) modeling approach based on seamless integration of multibody dynamics and the discrete element method (DEM) into one solver, and (ii) an HPC-based design-of-Experiments (DOE) approach to predict the off-road soft soil mobility of ground vehicles on large-scale terrain maps. A high-fidelity multibody dynamics model of a typical 4x4 military vehicle is used which includes models of the various vehicle systems such as chassis, wheels/tires, suspension, steering, and power train. A penalty technique is used to impose joint and contact constraints. A general cohesive soil material DEM model is used which includes the effects of soil cohesion, elasticity, plasticity/compressibility, damping, friction, and viscosity. To manage problem size, a novel moving soil patch technique is used in which DEM particles which are far behind the vehicle are continuously eliminated and then reemitted in front of the vehicle as new particles and then leveled and compacted. The governing equations of motion of both the vehicle and the soil particles are solved along with joint and contact constraints using an explicit time-integration procedure. The DEM inter-particle cohesion and friction forces are calibrated to the cone index using a simulation of a cone penetrometer experiment. The DOE approach is demonstrated by predicting the speed-made-good distribution for a typical military vehicle on 22 km × 22 km terrain map. Two terrain parameters are considered in the DOE, namely, terrain positive slope and soil strength. **This is the first time such mobility map is generated using high-fidelity physics-based simulations.***

1. INTRODUCTION

1.1 NRMM

Off-road vehicle mobility response on various terrains and for various vehicle configurations is of great importance to the Army as well as other departments of the military. Mobility measures include: speed-made-good (maximum speed of the vehicle in the desired direction while the vehicle is stable and under control), fuel consumption, and vibration power transmitted to the occupants/payloads. Currently the Army uses the NATO Reference Mobility Model (NRMM) [1, 2] to predict maps of the steady-state speed-made-good over terrains of interest for a given military vehicle type. NRMM was developed in the 1970's and is based on empirical relations to predict the vehicle mobility capabilities

on a given terrain unit while considering the following terrain variables: soil cone index (CI) [3, 4] (which is a measure of soil shear strength); surface cover (normal, water or snow); grade (uphill, downhill, and side); surface roughness; mound/trench obstacle size and spacing; tree/vegetation stem size and spacing; and visibility. The terrain empirical relations were tuned using 1960's to 1980's military vehicles. Those relations may not be accurate for new military vehicles such as: large vehicles with oversized wheels or tracks; small unmanned/robotic vehicles; vehicles with new airless tires or belt-type tracks; and vehicles with independent suspension or control technologies such as ABS, TCS, ESC, etc. This is due to the fact that those vehicles were not used to calibrate the empirical relations used in the current NRMM. Furthermore, those relations are difficult to generalize to the many types

and sizes of military vehicles, and conducting full-scale vehicle experiments to tune the NRMM empirical relations is very expensive and time consuming. The objective of this paper is to present a high-fidelity physics-based approach to accurately and reliably predict vehicle mobility maps over large off-road soft-soil terrains. The focus of the paper is on only two terrain variables: soil shear strength (measured by the CI) and terrain uphill grade. The rest of the terrain parameters such as side slope, negative slope, vegetation, obstacles, and visibility will be considered in future work.

1.2 Soft Soils

Soft soils can be divided into two main types: cohesive and non-cohesive. Cohesive soils include fine grained soils with high clay content (e.g. mud), and snow. Non-cohesive soils include dry sand and gravel. The main difference in mechanical response between cohesive and non-cohesive soil is that cohesive soils can support tensile forces, while non-cohesive soils cannot. For cohesive soils, soil strength is mainly due to normal adhesion forces between soil particles (i.e. particles stick together) which include: van der Waals forces and capillary liquid bridging forces. Thus, moisture content significantly affects the shear strength of cohesive soils. In this paper we will focus on cohesive soils. Cohesive soils have special mechanical characteristics [5-8] which make them challenging to model. Those include:

1. Soil bulk density increases with applied normal pressure (hydrostatic compressive stress). In addition, after removal of the applied normal pressure soil bulk density remains nearly unchanged. This implies that the soil underwent plastic deformation.
2. Soil shear strength increases with applied normal pressure. In addition, soil retains a significant portion of its shear strength after removal of the applied normal pressure. Thus, soil shear strength is a function of two parameters: the current applied normal pressure and the maximum previously applied normal pressure, also called consolidating stress. Figure 1 shows a typical plot of shear strength τ versus applied normal stress. B is the point where the applied normal stress is equal to the consolidating stress. The plot from point A to B can be used to draw Yield Mohr circles where the material cannot support the applied stresses and undergoes large shear deformation/flow. Soil shear strength can be attributed to two factors: adhesion between soil particles (cohesive forces) and tangential friction forces between soil particles. Soil adhesive/cohesive behavior is strongly affected by consolidation, while friction is not strongly affected by consolidation.

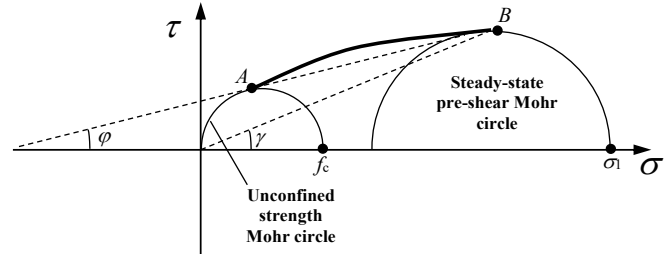


Figure 1. Yield locii and Mohr-Coulomb circles. σ is the applied normal stress and τ is the soil shear strength. f_c is the unconfined yield strength, σ_1 is the major consolidating stress, ϕ is the angle of internal friction, and γ is the effective angle of friction.

3. Soil shear strength and bulk density decrease when the soil is subjected to tensile forces above a certain limit. In other words when cohesive soil is subjected to significant tension soil particles become loose and the soil shear strength decreases.
4. Soil exhibits non-linear: elastic (normal force-deflection), damping (normal force versus deformation speed) and viscous (tangential force versus flow speed) mechanical behavior which is a function of the normal and consolidating stresses.

1.3 Physics-Based Models

High-fidelity techniques for modeling soft soils for vehicle mobility simulations can be divided into three groups based on the type of discretization: (1) height-field models; (2) finite element models; and (3) particle-based (mesh-free) models.

Height-field based models [9-15] divide the terrain into vertical cells. For each cell the soil height and state of normal and shear stresses are stored. If contact is detected between a cell and a tire or track tread element then the soil stresses and sinkage are calculated using the relative normal stress, tangential velocity, Bekker-Wong [5-7] or Janosi-Hanamoto [16] soil material models which calculate the shear stress in terms of the shear displacement, normal stress, shear modulus, cohesion, and angle of internal friction along with a Mohr-Coulomb shear failure criteria. This type of model was integrated into several multibody/vehicle dynamics software such as DADS [15] and SIMPACK [9-11, 17] for modeling vehicle mobility on soft soils. For example, in [9-11] a phenomenological terrain model was integrated in SIMPACK [17] where the soil surface was described using a “digital elevation map”, the wheel contact surface was represented as a point cloud, and an erosion algorithm was used to allow forming heaps in front of the wheels and side ruts. The main advantages of height-field terrain models is their computational speed and the fact that they are relatively simpler than other high-fidelity methods. Their disadvantages include: they are biased to the vertical direction (since they use a vertical sinkage field); they do not account for the

correct state of three dimensional deformation/stress in the soil; and ruts, heaps, and soil separation/reattachment effects are not accurately modeled. Their range of validity is generally limited to small soil deformation, where soil flow, bulldozing, and side ruts effects are negligible.

In finite element (FE) soil models [18-25] the soil is discretized into an FE mesh and an elasto-visco-plastic continuum mechanics constitutive material model [26] such as Drucker-Prager/Cap [27, 28] model is used to approximate the Mohr-Coulomb yield behavior of the soil (soil plastic yielding, internal friction, cohesion, and flow). Several commercial FE codes such as Abaqus [18-22, 29], PAM-CRASH [23, 30], and LS-DYNA [25, 31] include a Drucker-Prager/Cap type material model and have been used to simulate soil-wheel interaction. Most FE soil studies use a Lagrangian formulation where the soil deformation is modeled using the motion of the FE nodes. The main disadvantage of Lagrangian formulation is that if soil deformation is not relatively small remeshing is needed in order to avoid excessive element distortion. The remeshing step is computationally expensive and degrades solution accuracy since the solution fields (including plastic and deformations) need to be re-interpolated to the new mesh. Some FE studies used the Arbitrary Lagrangian Eulerian (ALE) formulation [18, 19] which allows mass transfer between elements to extend the range of soil deformation. However, even with ALE, effects such as soil bulldozing and separation/reattachment still require remeshing. In general, a cohesive soil continuum mechanics constitutive material model which accounts for the combined effects of material flow/fracture, plasticity, friction, and cohesion and the dependence of those properties on current stress and consolidation stress (or stress history) is still an open research problem. Wright [25], used the Eulerian formulation of LS-DYNA to model tire interaction with non-cohesive soil. The Eulerian formulation can handle soil flow and separation/reattachment with no need for remeshing. However, this study used a non-cohesive soil material model since a Drucker-Prager cohesive type material model was not available in LS-DYNA. In general, a cohesive soil material model which includes the combined mechanical behaviors of plasticity, friction, and cohesion is more difficult to implement within an Eulerian formulation than a Lagrangian formulation.

In particle-based models discrete particles are used to model the soil with inter-particle forces used to model the soil mechanical behavior. Particle models are the closest models to the actual physics of the soil. The main advantage of particle-based methods is their ability to naturally model material flow and separation/reattachment. Their main disadvantage is the large number of particles and high computational cost needed to accurately model the soil. There

are many particle based formulations that have been used to model soils in vehicle mobility simulations: DEM (Discrete Element Method), SPH (Smoothed Particle Hydrodynamics), MPM (Material Point Method).

In the DEM [32, 33] material behavior is modeled using inter-particle forces which include: normal contact forces (which can be deflection and/or velocity dependent) which prevent the particles from penetrating each other, attraction forces, tangential contact forces (including friction and viscous forces) and distance dependent forces (gravity, electrostatic and magnetic forces). DEM particles can have: only translational DOFs (i.e. point particles); or both translational and rotational DOFs (i.e. rigid body particles). Point particles are spherical, while rigid body particles can have arbitrary shapes (e.g. spherical, elliptical, or cubical). In [34, 35] spherical DEM particles were used to model soils in vehicle mobility applications. The inter-particle force model included particle stiffness and friction but did not include cohesive forces and plasticity. In [36], the DEM technique developed in [34, 35] was extended to non-spherical ellipsoid particles. In [37] a 2D DEM model that includes a tensile spring for accounting for soil cohesion was developed and used in soil-tire interaction simulations. In [38] the particle force model developed in [37] was implemented in a 3D DEM model and used to model a rigid wheel interaction with a cohesive soil. In [39-41] an implicit differential variational inequality (DVI) solver was developed and used in ground vehicle mobility simulations. The model included the effects of soil cohesion, friction, viscosity, and elasticity, but did not include plastic deformation and consolidation effects. In [42] a DEM cohesive soil material model was presented that can account for soil plasticity/bulk density, and cohesion including their dependence on normal stress and consolidating stress. In addition, the inter-particle force model also includes normal elastic and damping forces, and tangential friction and viscous forces. In [43] the model presented in [42] was extended to allow loss of cohesive strength due to tension using a time relaxation model of the soil plastic deformation. The DEM soil model developed in [42, 43] was integrated into the DIS [44] explicit multibody dynamics code and was demonstrated in full-vehicle mobility simulations over soil of various cohesions and terrains of various longitudinal and side slopes.

SPH [45, 46] is a mesh-free method where the particles are used as interpolation points for solving the continuum mechanics governing equations (Cauchy equation of motion in the case of soils). The continuum equations are discretized for each particle using a kernel smoothing function that is used to evaluate each particle properties and fluxes/forces acting on a particle using neighboring particles. In [47, 48] coupled FE tire model and SPH soil model created in PAM-CRASH [30] was used to simulate the rolling of rigid and

flexible tires on a soft soil. A hydrodynamic elastic-plastic material was used for the soil. The SPH model showed promise but it was concluded that the material models need to be further refined since they either showed excessive viscosity or incorrect material compressibility.

In the MPM [49] a Cartesian grid is used along with the particles to find neighboring particles as well as to discretize and solve the continuum mechanics governing equations. In [50] the MPM was used to model snow for computer graphics applications, including rigid body interaction, using a snow material model that includes stiffness, plasticity and fracture. In [51] MPM was used to model soil-structure interaction including pile driving and land-slides. A non-linear hypo-elastic sand material model was developed.

From the aforementioned literature review, it can be concluded that particle based methods are more suited for modeling soft soil which can undergo large deformation and material flow, including soil bulldozing, side ruts, and separation and reattachment effects. Accounting for those effects is necessary to be able to accurately predict vehicle mobility over soft soils. Of the particle methods, DEM is the most mature method for vehicle mobility applications. SPH and MPM rely on a continuum mechanics formulation, and therefore, they require a continuum mechanics cohesive soil constitutive material model, which as mentioned in the FE literature review is still an open research problem. In this paper the cohesive soil DEM formulation developed in [42, 43] is used along with a high-fidelity multibody vehicle dynamics model to predict the vehicle mobility over large terrain maps. A one-solver approach is used where the DEM and multibody dynamics are seamlessly integrated into one explicit time-integration solver. An HPC-based DOE procedure is used to generate the terrain mobility maps, considering two terrain variables, namely: CI and up-hill slope. Using a simulation of a cone penetrometer experiment, the CI is calibrated to the DEM soil model by varying the inter-particle cohesive/adhesive strength while using a fixed value for the inter-particle friction coefficient. This allows establishing a relation between NRMM and DEM practices.

The DOE procedure starts by dividing the terrain map into grid cells which are on the order of the size of the vehicle (typically 20×20 m). For each terrain cell the soil CI and maximum positive terrain slope is extracted, and hence, the ranges of terrain slope and CI for the entire map. Each variable is discretized into a number of values within the variable's range. Then, a vehicle mobility simulation is performed for each combination of discrete values of soil CI and terrain slope. All the combinations are run in parallel on individual HPC nodes and the various steady-state vehicle mobility measures are calculated. The mobility measures are then bi-linearly interpolated for each terrain grid cell and used

to color the cell. The coloring of the cells on the entire terrain map represents the mobility map. For example, Figure 2 which shows a typical speed-made-good map on a $22 \text{ km} \times 22 \text{ km}$ terrain map for a HMMWV-type vehicle generated using the present DOE procedure.

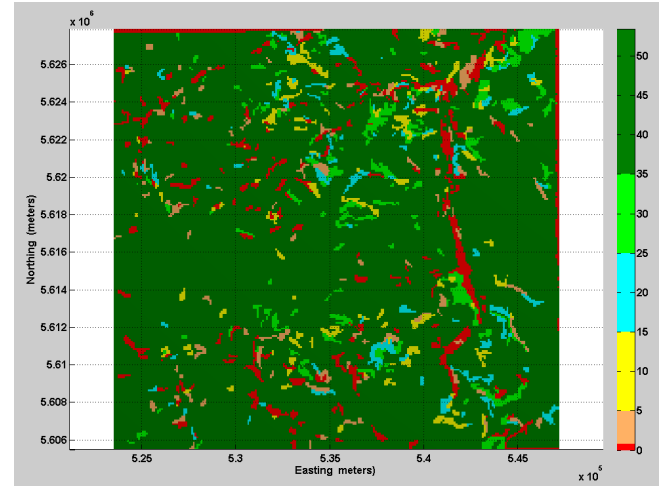


Figure 2. Terrain map ($22 \text{ km} \times 22 \text{ km}$) colored by speed-made-good in mph.

Vehicle speed over the terrain ranges from 0 (no-go) to the maximum vehicle speed (say 60 mph). In order to predict the speed-made-good over a terrain patch, the vehicle is commanded to slowly accelerate from rest to its maximum speed. Due to the combined resistances of the soil and terrain positive grade, the vehicle speed levels off below the commanded maximum speed, at which point the engine is applying the maximum available torque for the engine RPM. The actual steady-state maximum vehicle speed is the speed-made-good. Typically this requires a soil patch which is very long with millions of particles which can take months of simulation time. In order to perform the simulation in a reasonable amount of time (days), a **moving soil patch strategy** is used in this paper. This is achieved by only simulating the DEM particles which are close to the vehicle, and the particles which are far behind the vehicle are continuously eliminated and then reemitted as new particles in front of the vehicle. This ensures that the number of DEM particles remains manageable even for long vehicle travel distances.

The rest of this paper is organized as follows. In Section 2, an overview of the multibody vehicle dynamics and DEM cohesive soil models is presented. The cone penetrometer experiment model used to calibrate the DEM model to the CI is presented in Section 3. In Section 4, the vehicle mobility simulation model is described, along with the moving soil patch model. In Section 5, the DOE procedure is described. A

typical vehicle mobility simulation and map generated using the DOE procedure is presented in Section 6. The scalability of a vehicle mobility simulation on an HPC node is presented in Section 7. Finally, concluding remarks are presented in Section 8.

2. MODELING FORMULATION

The one-solver approach presented in [42, 43], which integrates: the finite element method (for modeling flexible vehicle components), multibody dynamics (for modeling vehicle rigid bodies and joints), and DEM (for modeling the soil) is used. A unified data structure is used where nodes can represent: FE nodes, rigid bodies, or soil particles. Two types of nodes are used: point nodes/particles which have 3 translational DOFs (degrees-of-freedom); and rigid-body type nodes which have 3 translational and 3 rotational DOFs. Point particles are used to model soil particles (as well as solid [52, 53], thin shell [54], and thin beam finite [55] elements) and (2) rigid bodies are used to model the vehicle rigid components (and can also be used to model rigid-body type soil particles). A node/particle is modeled as a point located at the particle's center of mass. The algorithm for writing and integrating the equations of motion for spatial rigid bodies using an explicit finite element code was presented in [56]. In the subsequent equations indicial notation is used and Einstein summation convention is used for lower case indices (which indicate coordinate numbers). The translational equations of motion for the nodes are written with respect to the global inertial reference frame and are obtained by assembling the individual node equations. The equations can be written as:

$$M_K \ddot{x}_{Ki} = F_{sKi} + F_{aKi} \quad (1)$$

where t is the running time, K is the global node number (no summation over K ; $K=1 \rightarrow N$ where N is the total number of nodes), i is the coordinate number ($i=1,2,3$), M_K is the lumped mass of node K , x is the vector of nodal Cartesian coordinates with respect to the global inertial reference frame, and \ddot{x} is the vector of nodal accelerations with respect to the global inertial reference frame, F_s is the vector of internal structural forces, and F_a is the vector of externally applied forces, which include surface forces and body forces.

For each rigid body/node, a body-fixed material frame is defined. The origin of the body frame is located at the body's center of mass. The mass of the body is concentrated at the center of mass and the inertia of the body is given by the inertia tensor I_{ij} defined with respect to the body frame. The orientation of the body frame is given by R'_K which is the rotation matrix relative to the global inertial frame at time t . The rotational equations of motions are written for each node with respect to its body fixed material frame as:

$$I_{Kij} \ddot{\theta}_{Kj}^i = T_{sKi}^i + T_{aKi}^i - \varepsilon_{ijk} \dot{\theta}_{Kj}^i (I_{Kkq} \dot{\theta}_{Kq}^i) \quad (2)$$

where I_{Kij} is the inertia tensor of rigid body K , $\ddot{\theta}_{Kj}$ and $\dot{\theta}_{Kj}$ are the angular acceleration and velocity vectors' components for rigid body K relative to its material frame in direction j ($j=1,2,3$), T_{sKi} and T_{aKi} are the components of the vector of internal and applied torques at node K in direction i of the local body frame and ε_{ijk} is the permutation tensor (to perform a cross product). Since, the rigid body rotational equations of motion are written in a body (material) frame, the inertia tensor I_{Kij} is constant.

The trapezoidal rule is used as the time integration formula for solving Eq. (1) for the global nodal positions x and Eq. (2) for the nodal rotation increments $\Delta\theta$:

$$\dot{x}_{Kj}^i = \dot{x}_{Kj}^{i-\Delta t} + 0.5 \Delta t (\ddot{x}_{Kj}^i + \ddot{x}_{Kj}^{i-\Delta t}) \quad (3a)$$

$$x_{Kj}^i = x_{Kj}^{i-\Delta t} + 0.5 \Delta t (\dot{x}_{Kj}^i + \dot{x}_{Kj}^{i-\Delta t}) \quad (3b)$$

$$\dot{\theta}_{Kj}^i = \dot{\theta}_{Kj}^{i-\Delta t} + 0.5 \Delta t (\ddot{\theta}_{Kj}^i + \ddot{\theta}_{Kj}^{i-\Delta t}) \quad (4a)$$

$$\Delta\theta_{Kj}^i = 0.5 \Delta t (\dot{\theta}_{Kj}^i + \dot{\theta}_{Kj}^{i-\Delta t}) \quad (4b)$$

where Δt is the time step. The trapezoidal rule is also used as the time integration formula for the nodal rotation increments $\Delta\theta$. The rotation matrix of body K (R_K) at time t is calculated using the rotation matrix at time $t - \Delta t$ and the rotation matrix corresponding to the incremental rotation angles $R(\Delta\theta_{Ki}^i)$:

$$R_{Kij}^t = R_{Kik}^{t-\Delta t} (R(\Delta\theta_{Kq}^i))_{kj} \quad (5)$$

The structural force (F_{sKi}) and torque vectors (T_{sKi}) can be a function of the position vector (x_{Kj}^i), velocity vector (\dot{x}_{Kj}^i), rotation matrix (R_{Kij}^t), and angular velocity vector ($\dot{\theta}_{Kj}^i$). The explicit solution procedure used for solving Eqs. (1-5) along with joint and contact constraint was presented in [42].

2.1 Joint Constraints

Joint constraints are imposed using a penalty formulation as presented in [42, 43, 56]. A joint connects two bodies by imposing kinematic constraints between points on the two bodies. For example, a spherical joint (Figure 3) between two points on two bodies is defined as:

$$x_{Ge1_i}^t = x_{Ge2_i}^t \quad (6)$$

where $x_{Ge1_i}^t$ is the global position of the first point on the first body and $x_{Ge2_i}^t$ is the global position of the second point on the second body. This constraint is imposed using the penalty technique:

$$F_c = k_p d + c_p \dot{d}_i d_i / d \quad (7a)$$

$$d_i = x_{Gc2i}^t - x_{Gc1i}^t \quad (7b)$$

$$\dot{d}_i = \dot{x}_{Gc2i}^t - \dot{x}_{Gc1i}^t \quad (7c)$$

$$d = \sqrt{d_1^2 + d_2^2 + d_3^2} \quad (7d)$$

$$F_{c_i} = F_c d_i / d \quad (7e)$$

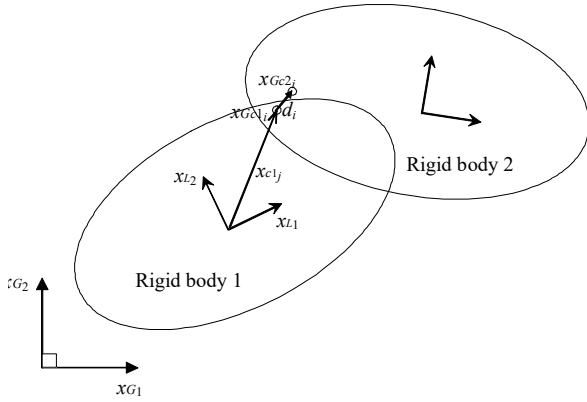


Figure 3. Spherical joint connecting two rigid bodies making two points x_{Gc1i} and x_{Gc2i} coincident.

where F_{c_i} is the penalty reaction force on the connection point, k_p is the penalty spring stiffness, c_p is the penalty damping, d_i is the relative displacement vector between points $c1$ and $c2$, and \dot{d}_i is the relative velocity vector between points $c1$ and $c2$. The constraint force is applied on the two connection points in opposite directions. Revolute joints can be modeled by placing two spherical joints along a line (Figure 4). A universal joint is modeled using 2 perpendicular revolute joints connecting 3 bodies (Figure 5). A bracket joints is modeled using 3 non-coincident spherical joints between two rigid bodies. Other types of joints such as cylindrical, prismatic, CV (Constant velocity), and gear joints can also be modeled by writing the constraint equation and then the corresponding penalty forces [43]. The constraint force F_{c_i} is transferred to the node at the center of the body as a force and a moment. The constraint forces are assembled into the global structural forces F_s in Eq. (1). The constraint torques are assembled into the global structural torques T_s in Eq. (2).

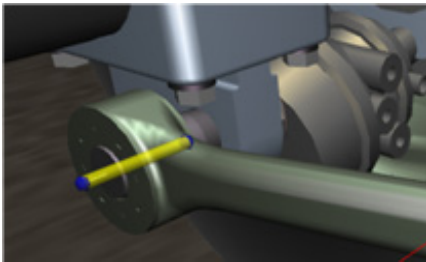


Figure 4. Revolute joint shown as a yellow cylinder is modeled using two spherical joints shown as blue spheres.

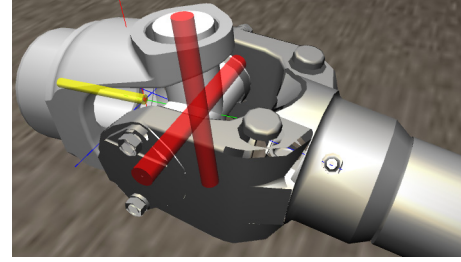


Figure 5. Universal joint is modeled using two perpendicular revolute joints shown as red cylinders connecting 3 rigid bodies.

2.2 Contact Constraints

The penalty formulation presented in [57-60] is used for modeling the contact constraints. Contact is modeled between a contact point on a rigid body/particle (master body) and a surface on another rigid body/particle (slave body) (Figure 6). After contact is detected, the contact point on the slave contact surface is found. The contact force vector F_{c_i} is divided into a normal force (F_{n_i}) and a tangential force (F_{t_i}) vectors:

$$F_{c_i} = F_{n_i} + F_{t_i} \quad (8)$$

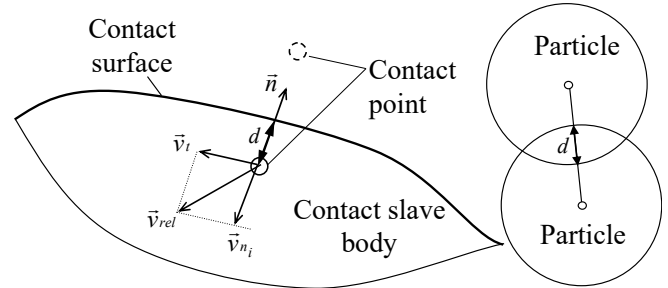


Figure 6. Contact surface and contact point, and particle to particle contact. d is the penetration.

The normal and tangential contact force vectors are given by:

$$F_{n_i} = n_i |F_n| \quad (9)$$

$$F_{t_i} = t_i |F_t| \quad (10)$$

where n_i is the surface normal unit vector, t_i is a unit vector along the tangential velocity direction, and $|F_n|$ and $|F_t|$ are the magnitudes of the normal and tangential forces, respectively. $|F_n|$ is calculated using:

$$|F_n| = F_{repulsion} + F_{damping} \quad (11)$$

where $F_{repulsion} = k_n d$ (12a)

$$F_{damping} = \begin{cases} c_n \dot{d} & \dot{d} \geq 0 \\ s_n c_n \dot{d} & \dot{d} < 0 \end{cases} \quad (12b)$$

where $F_{repulsion}$ is the repulsive force, k_n is the normal contact surface penalty stiffness, $F_{damping}$ is the normal damping force, c_n is the penalty damping coefficient, and s_n is a separation damping factor (typically between 0 and 1) which reduces normal damping when the two bodies are moving apart. Note that k_n and c_n can be specified as a function of d and \dot{d} . This allows modeling various types of Hertzian contact. $|F_t|$ is calculated using:

$$|F_t| = F_{viscous} + F_{friction} \quad (13)$$

where $F_{viscous}$ is the viscous force and $F_{friction}$ is the friction force. $F_{viscous}$ is given by:

$$F_{viscous} = c_t |v_t| \quad (14a)$$

where: $|v_t| = \sqrt{v_{t_x}^2 + v_{t_y}^2}$ (14b)

c_t is the viscosity coefficient and $|v_t|$ is the signed tangential velocity magnitude. An asperity friction model is used along with the normal repulsive ($F_{repulsion}$) force to calculate the tangential friction force ($F_{friction}$) [58]. In this model, friction is modeled using a piece-wise linear velocity-dependent approximate Coulomb friction element in parallel with a variable anchor point spring. The model approximates asperity friction where friction forces between two rough surfaces in contact arise due to the interaction of the surface asperities. The contact model is used to model contact between the tire (master) and hard pavement surface (slave).

2.3 DEM Cohesive Soil Model

In this section we will derive expressions for the normal force $|F_n|$ and tangential force $|F_t|$ for modeling cohesive soils and soil contact with vehicle surfaces (such as tires, wheels and track segments). $|F_t|$ is calculated using Equation (13). The viscous force is given by Equation (14) and the friction force is calculated using the aforementioned asperity friction model. $|F_n|$ is calculated using:

$$|F_n| = F_{adhesion} + F_{repulsion} + F_{damping} \quad (15)$$

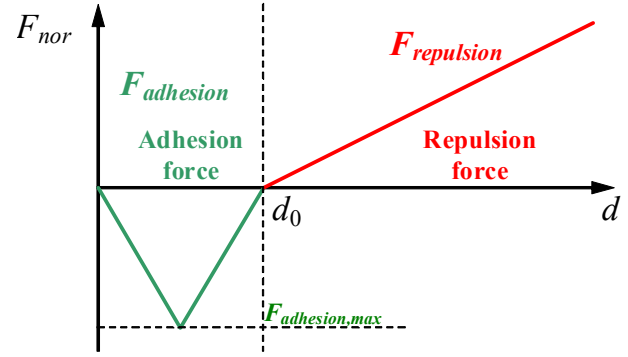


Figure 7. Normal adhesive and repulsive contact forces.

The normal damping force ($F_{damping}$) is given by Equation (12b). $F_{adhesion}$ and $F_{repulsion}$ are both specified as a function of contact point penetration into the contact surface d (Figures 6 and 7). Up to a penetration distance d_0 the contact forces are attractive. A force greater than $F_{adhesion,max}$ is needed to separate the two bodies. If the penetration exceeds d_0 then the contact force becomes repulsive thus opposing further penetration. The adhesive force along with the friction force contribute to the cohesive strength of the soil. Note that the adhesive and the repulsive force can be a non-linear function of the penetration distance. The actual shape of the curve in Figure 7 can be tuned using experimental data.

In order to model the permanent plastic deformation of the soil, plastic deformation ($\delta_{plastic}$) can be specified as a function of repulsive (compression) force ($F_{repulsion}$). For example, Figure 8 shows a typical particle plastic strain curve versus compressive stress. The $\delta_{plastic}$ versus $F_{repulsion}$ curve can be tuned to match the bulk density versus consolidating pressure curve for the soil (e.g. Figure 9) obtained from using piston-cylinder soil uniaxial compression experiment.

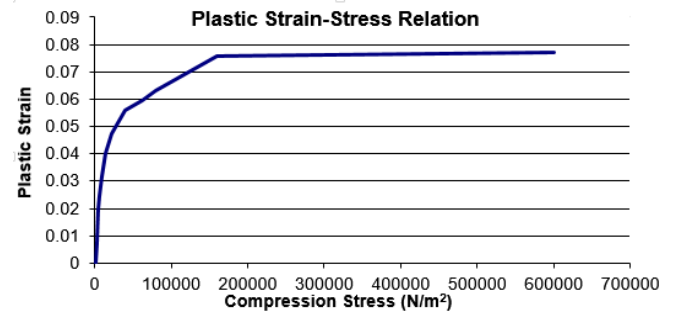


Figure 8. Typical curve of particle plastic strain as a function of compressive stress.

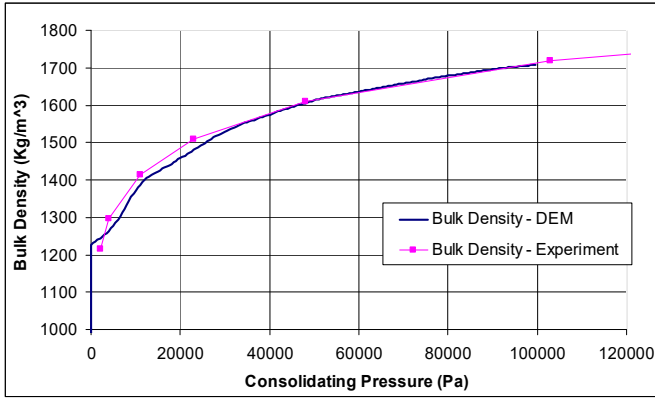


Figure 9. Typical bulk density versus normal pressure curve for a cohesive soft soil - comparison of experiment data and tuned DEM model.

In order to account for the increase in soil cohesive strength of consolidated soil, the maximum adhesive force ($F_{adhesion,max}$) in Figure 7 is specified as function of the plastic deformation. For example, Figure 10 shows a typical maximum adhesion stress versus plastic strain for a DEM particle. The friction coefficient (μ), viscosity coefficient (c_n) and damping coefficient (c_i) can also be specified as a function of the plastic deformation ($\delta_{plastic}$). The curve in Figure 10 along with the friction coefficient can be tuned to match the shear stress versus normal stress for different consolidation normal stress values obtained using a shear cell [8]. An example of a typical shear stress versus normal stress curve for one value of consolidation normal stress is shown in Figure 1.

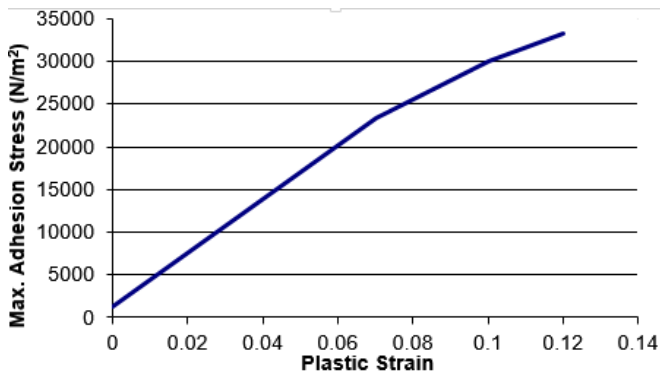


Figure 10. Typical maximum adhesive stress versus plastic strain curve.

In order to account for the reduction of soil cohesive strength and soil bulk density due to tension and/or removal of the compression, a time relaxation is applied to the soil plastic deformation each time step:

$$\delta_{plastic} = \delta_{plastic} - \begin{cases} 0 & F_{repulsion} \geq F_{adhesion,max} \\ V_{relax} \times \Delta t & F_{repulsion} < F_{adhesion,max} \end{cases} \quad (16)$$

where V_{relax} is the speed of plastic relaxation (in distance/time) and Δt is the explicit solution time step. Thus, if the particle's repulsive (compressive) force (maximum force value over all adjacent particles) is larger than the maximum adhesive (tensile) force then the particle plastic deformation is left unchanged. If the particle repulsive force is smaller than the maximum adhesion force then the particle plastic deformation is reduced at a speed of V_{relax} . The smallest allowable plastic deformation value is zero. The value of V_{relax} is experimentally tuned.

The DEM force model presented in this section is used as the inter-particle force model for soft cohesive soils. The force model can be tuned to a particular soil material using the following experiments:

- Piston-cylinder uniaxial compression apparatus for measuring the soil bulk density versus consolidating pressure (Figure 9).
- Shear apparatus [8] for measuring the soil cohesive strength and internal friction as a function of consolidation pressure and applied normal pressure (Figure 1).
- Penetrometer can also be used to tune the soil cohesive strength and inter-particle friction coefficient. However, the consolidation pressure and applied normal pressure cannot be applied independently. This makes this experiment only suitable for model verification.
- Angle of repose of a material pile can be used to tune the unconsolidated (loose) soil cohesive strength and inter-particle friction coefficient.
- Flow rate from hoppers can be used to tune the soil cohesive strength, inter-particle friction coefficient and wall adhesion.
- Wall material shear apparatus can be used to tune the friction and adhesion to wall materials.
- Blade-soil experiments measuring the blade speed, drawbar force, normal force, and sinkage. This experiment can be used to tune/verify the soil cohesive strength, inter-particle friction coefficient and plastic relaxation speed.
- Wheel-soil experiments measuring torque, angular velocity, speed, drawbar force, normal force and sinkage. This experiment can be used to verify/tune the soil cohesive strength and inter-particle friction coefficient.

The force model can also be used as the particle-wall force model to model the contact between the particle and other solid bodies. The force model can be tuned to particular soil and wall materials using a shear apparatus for measuring wall friction.

3. CONE PENETROMETER SIMULATION FOR RELATING NRMM AND DEM PRACTICES

A model of the standard cone penetrometer experiment is created using DIS [44] and used to calibrate the cone index (CI) used in NRMM with the parameters of the DEM soil material model presented in Section 2.3. Note that NRMM uses the rating cone index (RCI) for cohesive soils which is the CI of the consolidated/compressed soil [4]. Therefore, the soil in cone penetrometer as well as the vehicle mobility simulations is consolidated to the initial strength using a lid which applies the consolidation pressure. The two DEM model parameters which directly affect the CI and which will be tuned using the cone penetrometer experiment model are the maximum DEM adhesion and the inter-particle friction coefficient (μ). Figure 11 shows the model of the cone penetrometer experiment. The model consists of three rigid bodies: ground (cylindrical soil container), the cone penetrometer, and a flat lid. The values of the parameters of the experimental setup are shown in Table 1. The values of the parameters of the DEM cohesive soil model are shown in Table 2. The total number of soil particles is more than 300,000. The explicit integration time step is 1.5×10^{-5} sec. The experiment starts by dropping the soil particles into the cylindrical container. Then, the lid is used to consolidate the soil up to a pressure of 33.3 kPa for 0.5 sec, after which the lid is removed. Then, the cone penetrometer is moved downward at a constant speed of 0.1 m/s using a PID controller. We record the value of the CI as the steady-state penetration force divided by the base area of the cone penetrometer in psi.

The CI is tuned by varying two DEM parameters: the maximum adhesion stress and the friction coefficient (μ). The nominal maximum adhesion stress versus plastic strain curve is shown in Figure 10. This curve is scaled by a factor between 0.05 and 12, with 1 corresponding to the nominal curve in Figure 1. We call this scale the “cohesion factor (f).” μ is varied from 0.05 to 0.1. The ranges of f and μ are chosen such that the range of cone index for the sample terrain used in the numerical study in Section 5 is between 30 to 300 psi. Figure 12 shows typical snapshots of a cross-section of the cone penetrometer experiments for a low-cohesion and a high-cohesion soil. Figure 13 shows the CI versus time for different values of f for $\mu = 0.1$. Figure 14 shows a plot of the CI versus cohesion factor for $\mu = 0.05$ and 0.1. Since the focus of this paper is on cohesive soils, we will fix μ at 0.1 and vary only f to tune to the value of CI. A third order polynomial is used to map f to the CI for inter-particle coefficient of friction 0.1:

$$f = 9.148 \times 10^{-7} CI^3 - 1.783 \times 10^{-4} CI^2 + 4.555 \times 10^{-2} CI - 1.445$$

The above equation is then used to map CI to f (Table 3) which will be used in the vehicle mobility simulations.

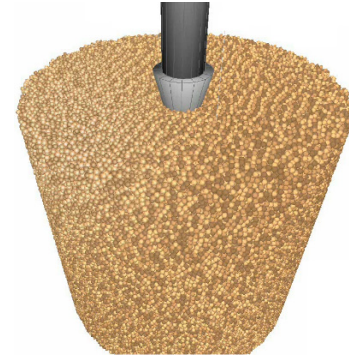


Figure 11. Model of the cone penetrometer experiment.

Table 1. Parameters of the cone penetrometer experiment.

Cylindrical container diameter	2 m
Consolidating lid pressure	33.3 kPa
Cone penetrometer base diameter	0.375 m
Cone penetrometer length	0.7 m
Cone penetrometer cone angle	30°
Penetrometer speed	0.1 m/s

Table 2. Parameters of the DEM soil particles.

Unstressed (unconsolidated) particle diameter	0.03 m
Particle mass density	1800 kg/m ³
Inter-particle friction coefficient	0.1
Particle to tire/cone penetrometer friction coefficient	0.5
Inter-particle viscosity	0
Inter-particle damping per unit area	2.1×10^4 N/m ³ /s
Particle stiffness (slope of repulsion stress versus penetration strain in Figure 7)	4.42×10^7 N/m ²
Plastic strain versus compressive stress	Figure 8
Nominal maximum adhesion stress versus plastic strain curve	Figure 10
Plastic relaxation speed	0.045 m/s

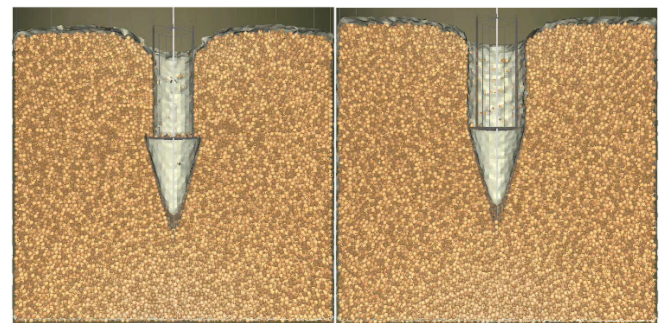


Figure 12. Snapshots of a cross-section of the cone penetrometer experiment for inter-particle coefficient of friction of $\mu = 0.1$ and cohesion factors (f) of 0.05 and 12 that correspond to a CI of about 30 and 240, respectively.

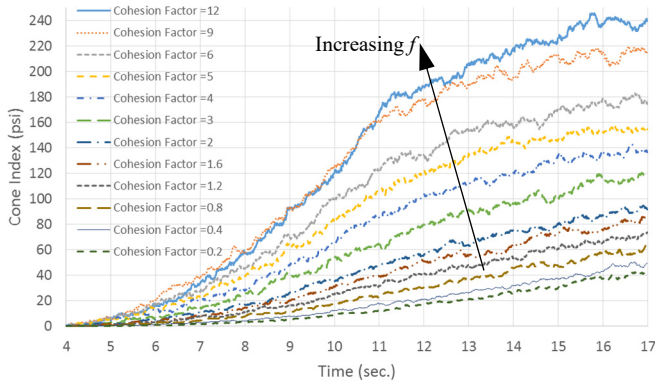


Figure 13. CI versus time for different values of soil cohesion factor (f) and $\mu = 0.1$.

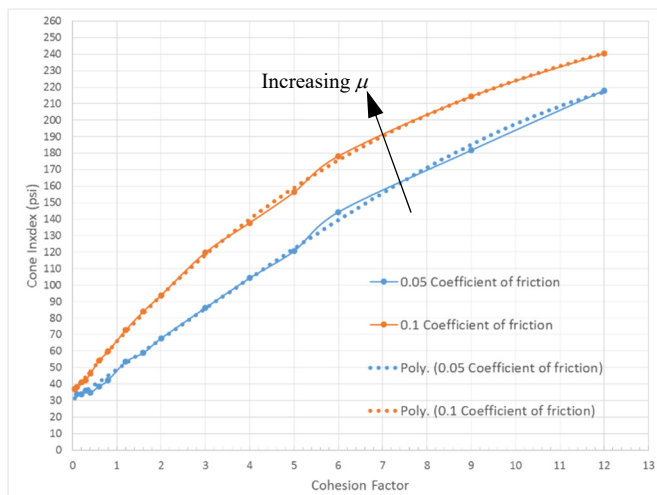


Figure 14. CI versus cohesion factor (f) for $\mu = 0.05$ and 0.1 .

Table 3. Polynomial fit of cone index (CI) versus cohesion factor (f) for $\mu = 0.1$. Note that for CI = 300, no DEM soil is used and the soil is modeled using a polygonal surface with appropriate normal stiffness/damping and friction coefficient.

	Cone Index	Polynomial Fit Cohesion Factor
1	30	0.06
2	40	0.15
3	50	0.5
4	60	0.84
5	70	1.18
6	80	1.52
7	100	2.24
8	120	3.03
9	150	4.46
10	200	7.85
11	242	12.1
12	300	Polygonal road

4. VEHICLE MOBILITY SIMULATION MODEL

In this section, we describe the multibody dynamics vehicle model and the moving DEM soil patch model. A parallel explicit solution procedure is used to solve Equations (1-6) along with the constraint equations [42, 43] and is implemented in DIS [44] which is used to create the integrated multibody dynamics - DEM model and to generate the simulation results.

4.1 Vehicle Model

Figure 15 shows the vehicle multibody dynamics model. It consists of 33 rigid bodies: main chassis; 4 wheels; 4 upper suspension control arms; 4 lower suspension control arms; 4 knuckles; 6 bodies for the front axle; 6 bodies for the rear axle; drive shaft; 2 tie rods; and steering rack. The bodies are connected using spherical, revolute, prismatic and CV joints. A gear differential model [43] is used to model the front and rear differentials. A rotational actuator is used to model the drive torque at the drive shaft (tractive torque after the transmission system). The torque is limited to be between the two curves shown in Figure 16 which represent the WOT (wide-open throttle) torque shown in blue and the maximum engine brake torque shown in purple, as a function of the drive shaft angular velocity. Four rotational actuators at the wheels are used for modeling the brakes. The maximum brake torque as a function of the wheel angular velocity is shown in Figure 17. A braking effort between 0 and 1 multiplies by the maximum brake torque to determine the value of the applied brake torque. The total sprung mass of the vehicle is 4,430 kg. The mass of one wheel is 50 kg. Each tire polygonal surface consists of more than 6600 triangles (Figure 15). The tire diameter is 0.97 m. The tires' surfaces are set as slave contact surfaces for the DEM particles. The tires are modeled as rigid in this paper.

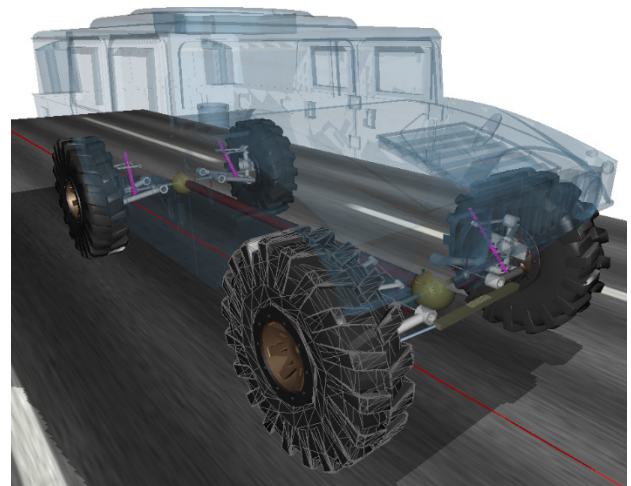


Figure 15. Multibody dynamics model of the HMMWV-type vehicle.

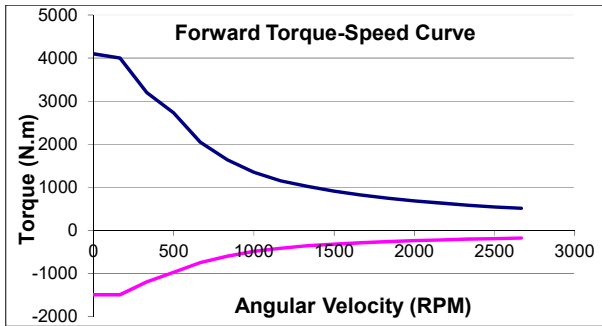


Figure 16. WOT engine torque shown in blue and maximum engine brake torque shown in purple, after the transmission system.

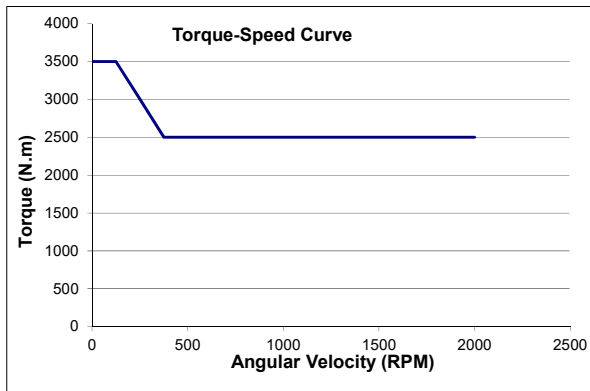


Figure 17. Maximum brake torque at each wheel.

4.2 Soil Model

The DEM soil material properties are listed in Table 2. The DEM model has about 620,000 point-type particles with an undeformed particle diameter of 3 cm. The soil particles are inside a bounding box that is 9.3 m long, 3.5 m wide, and 0.9 m high with an open top (Figure 18). The soil is compressed in the vertical direction using a flat lid for one second using a pressure of 33.3 kPa. The lid is removed after the consolidated soil settles to a height of about 0.4 m. A Cartesian search grid with a resolution of 310 (length), 116 (width) and 30 (height) is used. The side length of a grid cell was chosen to be almost equal to the diameter of the particle.

A moving soil patch technique is used in which the particles which are far behind the vehicle are continuously eliminated and then reemitted as new particles in front of the vehicle. This is achieved using a rectangular particle emitter, a leveling cylinder and plate, and a bounding sphere (see Figure 18). When a particle goes outside the bounding sphere it is deactivated and then immediately reemitted as a new particle from the rectangular particle emitter from a random point on the surface of the emitter. Once the x-coordinate of the c.g. of the vehicle reaches initial x-coordinate of the center of the bounding sphere, then the bounding sphere center is moved

with the c.g. of the vehicle frame using a script function along with a prescribed motion constraint.

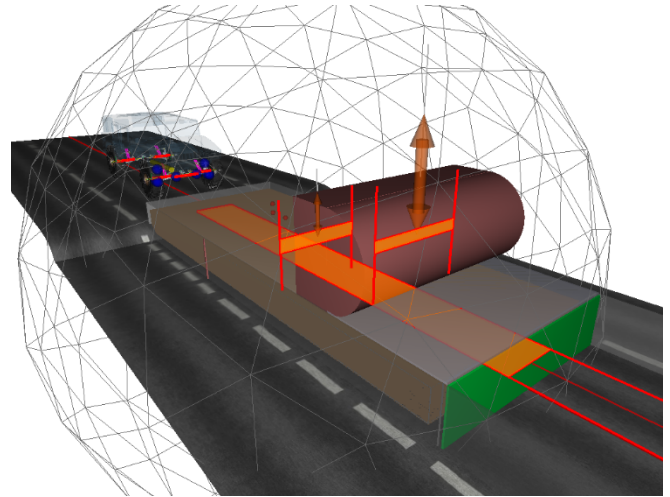


Figure 18. Moving soil box model consisting of a moving box, a leveling lid, a leveling cylinder/plate (shown in red), and a rectangular particle emitter (shown in green).

The moving soil patch technique ensures that the number of DEM particles remains relatively small for long vehicle travel distances, and that the simulation can complete in a reasonable amount of time. To reach its maximum speed of 60 mph from rest and run a few seconds at steady-state, the vehicle needs about 400 m long terrain patch. If the patch width is 3.5 meters, consolidated soil depth is 0.4 meters, and consolidated particle diameter is 26.5 mm, then the required number of particles is about 67,000 particles per meter of terrain. So for a 400 m long terrain patch about 27 million particles are needed. At current simulation computational speeds, a 40 sec simulation with 27 million particles will take about 9 months to complete. However, for the simulations in this paper where the moving terrain patch is 9.3 m long and the number of particles is about 620,000, a 40 sec vehicle simulation takes about 7 days on a 32 core HPC node.

4.3 Simulation Scenario

In the vehicle mobility simulation, the terrain and soil patch are set to a desired grade, and the soil is set to a desired cone index (by specifying the inter-particle friction coefficient and cohesion factor) in the pre-processor. Then, the simulation starts by leveling and consolidating the soil using a flat lid, then the leveling cylinder and plate are lowered to the initial height of the soil (about 0.4 m). Next the vehicle is commanded to accelerate at 1 m/s² from rest to a maximum speed of 25 m/s (56 mph) in 25 sec. Due to the soil and grade resistances, the vehicle speed levels off below the commanded maximum speed, at which point the engine is applying the maximum available torque (at the running

engine RPM). Note that the vehicle may need longer time than the desired 25 sec to accelerate to its maximum steady-state speed (due to the fact that the available engine torque is not sufficient to accelerate the vehicle at the desired acceleration). So, the total simulation time is set to 40 sec. The steady-state maximum vehicle speed in the desired travel direction is the speed-made-good and the rest of the vehicle mobility measures are also extracted at this steady-state.

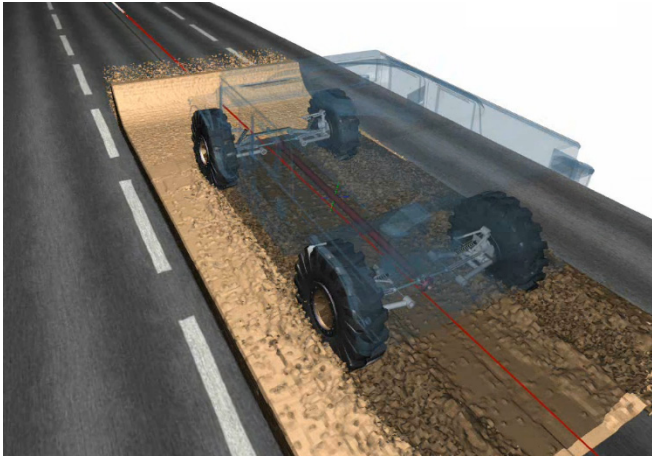


Figure 19. Snapshot of a typical simulation of the coupled HMMWV multibody vehicle dynamics and DEM soil moving terrain patch models.

5. VEHICLE MOBILITY DOE PROCEDURE

The DOE procedure used to predict the “speed-made-good” and other mobility measure distributions over large terrain maps consists of the following steps:

1. The rectangular terrain map of 22 km x 22 km is divided into 20 m x 20 m grid cells. For each grid cell the maximum slope and the minimum soil cone index are extracted. Then, the ranges of such slopes and cone indices for the entire terrain map are found.
2. The positive slope range of the terrain map is discretized into a certain number of values (G). Also, the CI range is discretized into a certain number of values (C). Then a vehicle mobility simulation is performed for each of the $G \times C$ combination of slope and cone index. All the combinations are run in parallel on individual HPC node. For each combination, the various steady-state vehicle mobility measures are calculated. Then the mobility measure values are bi-linearly interpolated from the calculated values to the actual values for each terrain grid cell.
3. A map of the mobility measure over the entire terrain map is then generated by coloring each grid cell using the mobility measure (such as the speed-made-good).

In developing the mobility map for this research, the number of HPC runs made was 168 ($G = 14 \times C = 12$). Each run takes a maximum of 7 days to run on an HPC node. Therefore, the theoretical required computer time is 1176 days. Note that since all the runs are performed in parallel, the actual time to get the results is 7 days. Also note that for about half of the runs (high-slope and low CI runs), the vehicle speed-made-good (mobility) is zero and the simulations can be ended well before the full 40 sec. Without the DOE procedure, a separate run would be required for each terrain cell. The 22 km x 22 km would require $1100 \times 1100 = 1.21$ million runs instead of 168.

Also, note that the simulations are performed for the positive slope since this will typically result in the worst possible vehicle mobility while crossing a terrain, which is what mission planners are most interested in. Even, if the actual vehicle motion direction is not along the maximum longitudinal slope direction, due to obstacles or mission uncertainties it is possible that the vehicle may need to move along the maximum positive slope direction. Mission planners are also interested in the directional mobility maps (also called traverse map). Creating a DOE to generate those mobility maps will be the subject of future research.

6. VEHICLE MOBILITY RESULTS

In this Section, the DOE procedure described in Section 5, is used to generate a vehicle mobility map for a 22 km x 22 km rectangular terrain map. The terrain map is divided into 20 m x 20 m rectangular cells. The range of slopes for the cells is from 0 to 39 degrees (80% grade). This range is discretized into 14 values 0, 3, 6, ... 36, 39°. The range of CI is 30 to 300 and is discretized using the 12 CI values in Table 3. A vehicle simulation is performed for each combination of longitudinal slope and CI. Note that for about half-of the runs, the vehicle gets stuck (i.e. speed-made-good is zero) after a few seconds of the simulation, due to the combined effect of high slope and low soil cohesion. Once the vehicle gets stuck then the run can be ended. Snapshots of 4 combinations of soil CI and terrain slope simulations are shown in Figure 20.

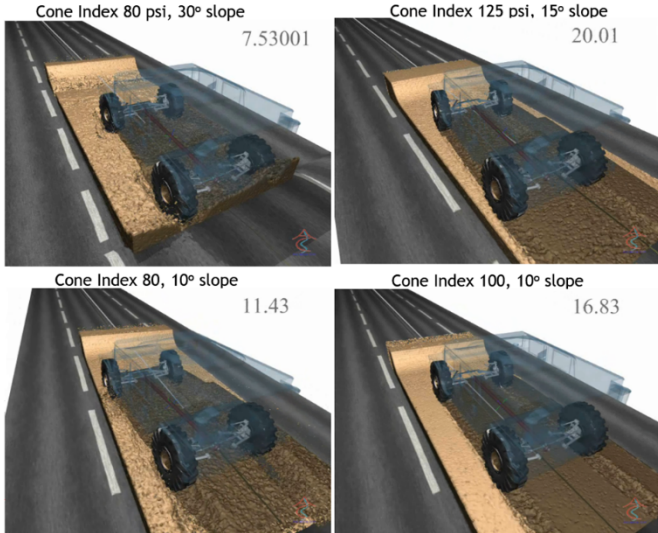


Figure 20. Snapshots of a HMMWV-type vehicle going over terrains of various slopes and cone indices.

Figures 21 and 22 show plots of the vehicle speed time-history for terrain slopes 0 and 6°. As seen in the figures, the vehicle is commanded to accelerate to 25 m/s at 25 sec, but due to soil and grade resistances and available engine torque, the vehicle steady-state speed is reached after more than the commanded 25 sec and is less than the maximum commanded speed. Also, from the figures, the vehicle speed increases with CI and decreases with slope.

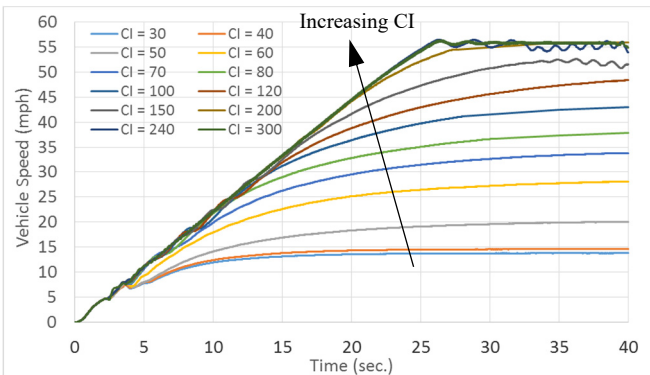


Figure 21. Physics-based model’s vehicle speed time-history for CI = 30 to 300 psi and terrain slope 0°.

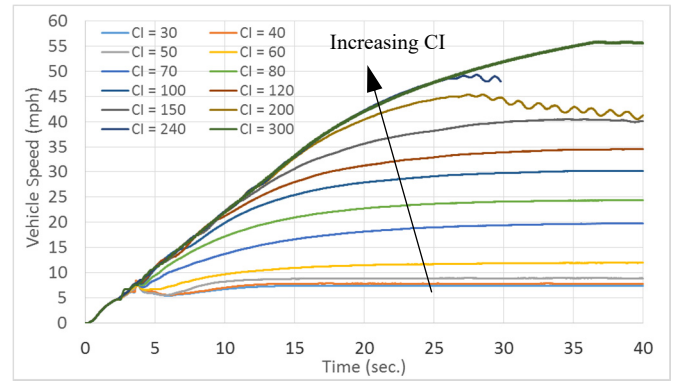


Figure 22. Physics-based model’s vehicle speed time-history for CI = 30 to 300 psi and terrain slope 6°.

Figures 23 and 24 show the steady-state vehicle speed (speed-made-good) as function of CI and terrain slope, predicted by the physics-based model and NRMM software [1, 2], respectively. In the NRMM results, all speed limiting factors were eliminated except for positive terrain slope and CI. The figures show that the results from NRMM and the physics-based model are different. For example, extracting the results for the 12° sloped terrain from the Figures 23 and 24, the physics-based model predicts that the vehicle will have zero mobility for soils of CI = 30 to 80. Then, the vehicle speed-made-good increases until it levels off at about 40 mph at CI = 200. NRMM predicts that the vehicle speed-made-good is about 7 mph for CI = 30, then it increase to about 15 mph at CI = 70, after which it remains nearly constant up to CI = 300. Figures 25 and 26 show a comparison of mobility maps for the same 22 km × 22 km terrain map generated by the physics-based model and NRMM that are distinctly different. The difference in results between the physics-based model and NRMM can largely be due to the inaccuracies of NRMM and a lack of experimental data for calibration of the physics-based model. These topics will be the subject of future research.

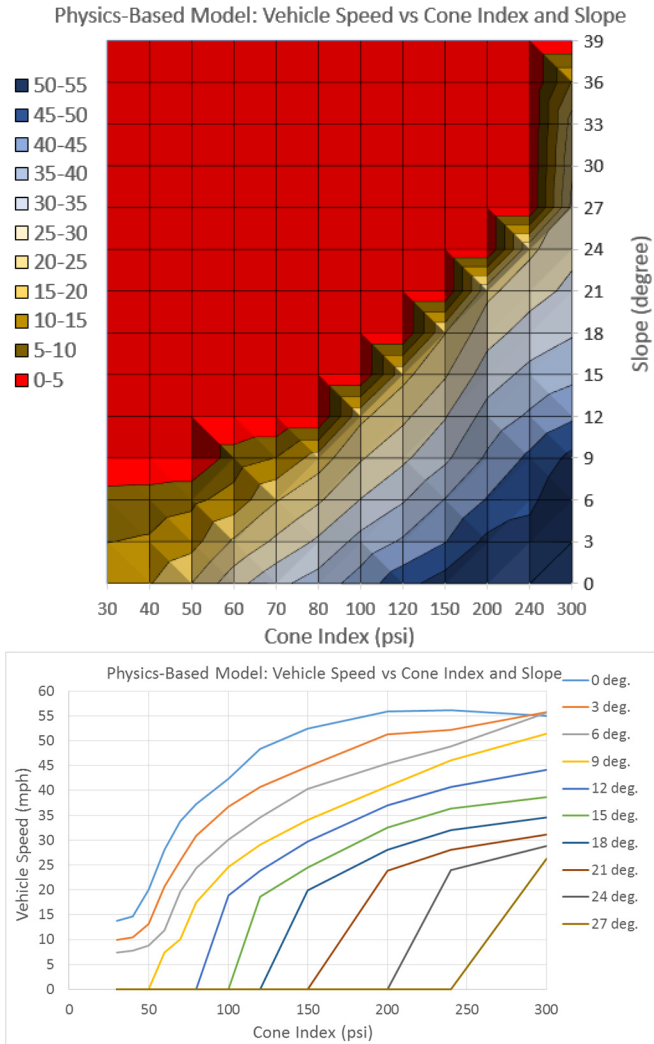


Figure 23. Physics-based model’s steady-state vehicle speed (speed-made-good) versus CI and terrain slope. Note that the same data is shown in the top and bottom figures. The top figure shows a color map of vehicle speed as a function of CI and terrain slope. The bottom figure shows plots of CI versus vehicle speed for different terrain slopes.

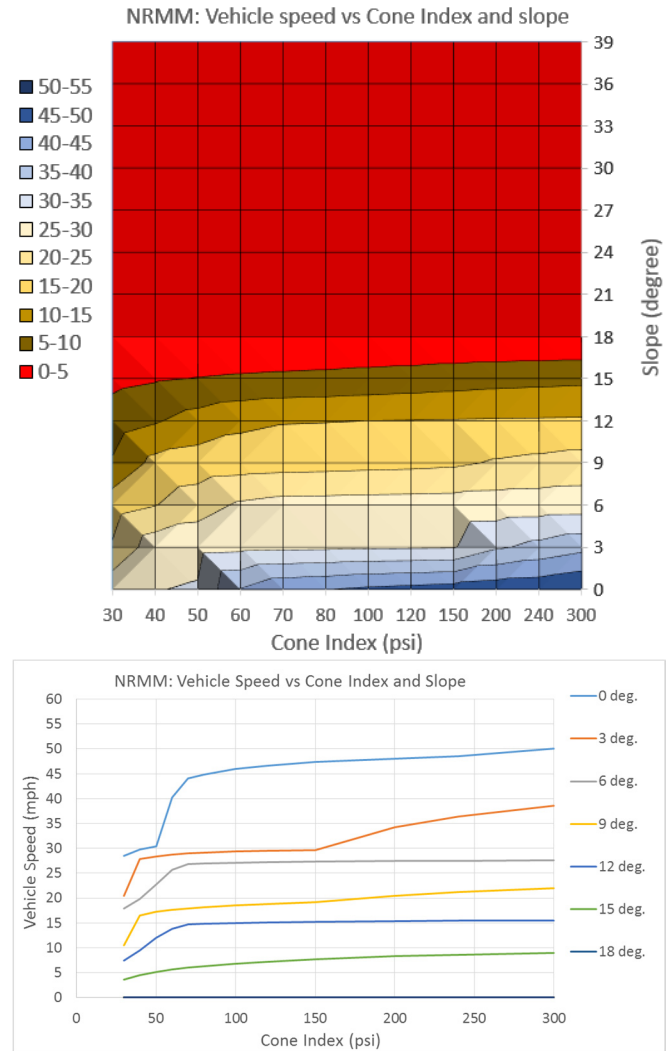


Figure 24. NRMM speed-made-good versus CI and terrain slope.

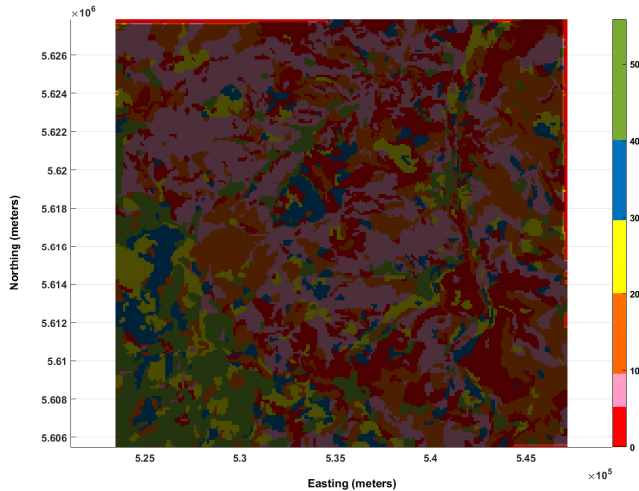


Figure 25. A 22 km x 22 km mobility map in mph generated using the physics-based model.

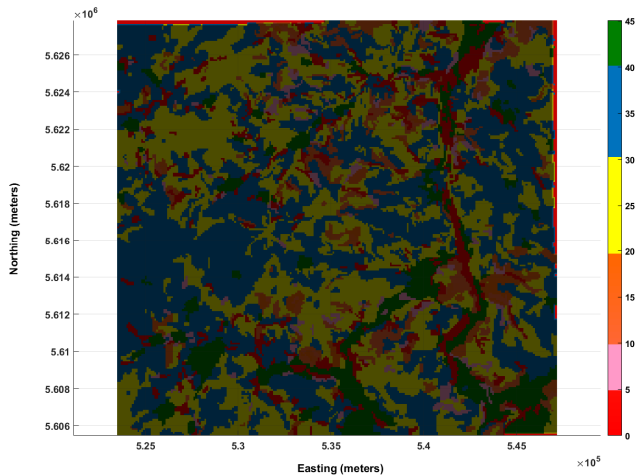


Figure 26. A 22 km x 22 km mobility map in mph generated using NRMM.

7. SCALABILITY OF THE SIMULATIONS

The vehicle mobility simulation is performed on one shared-memory HPC node in parallel on the node's cores by running the internal force calculations (for the DEM particles and the vehicle joints and contact surfaces) and the time integration for the DEM particles and vehicle rigid bodies, in threads which run on parallel on the available node's cores. The number of threads is set equal to the number of cores, so that each thread runs on one core. All the cores/threads share the same computer memory (shared-memory parallel processing). Figure 27 shows the computational speed in simulation seconds per second of real time for a typical vehicle mobility simulation on one node of an HPC versus the number of cores used. The HPC is a Cray XC40 belonging to the DOD Supercomputing Resource Center (DSRC) located at the Army Research Laboratory (ARL). The HPC node has

2 Intel Xeon E5-2698 v3 2.3 GHz CPUs with 16 cores each for a total of 32 cores per node. Initially, the computational speed increases nearly linearly with the number of cores, but levels off after about 16 cores due to memory access bottlenecks (all the threads are trying to access the memory bus at the same time). The computational time was about 15,000 sec per second of simulation for 16 cores, while it was about 12,800 sec for 32 cores.

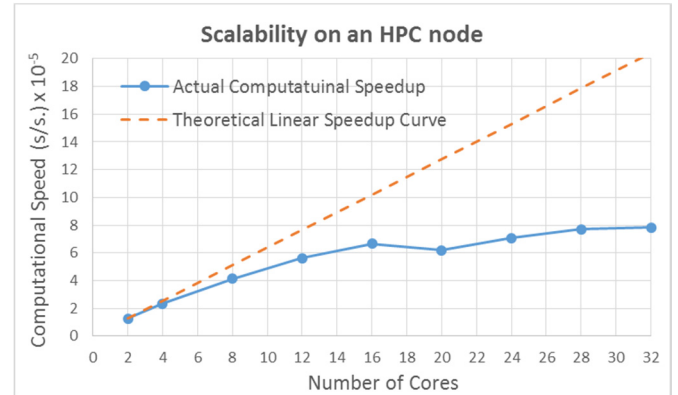


Figure 27. Computational speed (seconds of simulation per real-time seconds) for a typical vehicle mobility simulation on a DSRC HPC node versus the number of cores.

8. CONCLUDING REMARKS

For the first time, a high-fidelity physics-based simulation to reliably predict vehicle mobility measures over large terrain maps was presented. The modeling approach is based on: (i) seamless integration of multibody dynamics for modeling the vehicle and DEM for modeling cohesive soils into one solver; (ii) an HPC-based DOE procedure to predict the off-road soft soil mobility of ground vehicles on large-scale terrain maps; and (iii) a moving terrain patch strategy to reduce the DEM problem size and simulation time. This approach is proposed to replace the current practice of NRMM that is known to be inadequate. The resulting mobility maps highlight the differences between the two approaches. Future work will focus on expanding the DOE procedure to include additional terrain and soil properties as well as devising calibration and validation experiments for the physics-based model.

ACKNOWLEDGEMENTS

The authors acknowledge the financial support from the U.S. Army TARDEC through (i) Contract # W911NF-11-D-0001-0311 for the first author, and (ii) F22 Mobility Research funds for the U.S. Army TARDEC authors.

The authors would like to thank Dr. David Lamb of the U.S. Army TARDEC and Charlie Nietubicz of Battelle for

securing access to the Dedicated Support Partition (DSP) in the ARL DSRC HPC computers.

The authors also would like to thank John Green of the U.S. Army Engineer Research and Development Center (ERDC) for providing NRMM support and terrain data.

Disclaimer: Reference herein to any specific commercial company, product, process, or service by trade name, trademark, manufacturer, or otherwise does not necessarily constitute or imply its endorsement, recommendation, or favoring by the United States Government or the Dept. of the Army (DoA). The opinions of the authors expressed herein do not necessarily state or reflect those of the United States Government or the DoA, and shall not be used for advertising or product endorsement purposes.

REFERENCES

- Ahlin, R. and P. Haley, *NATO Reference Mobility Model Edition II, User's Guide*, in *Technical Report Number GL-92-19, U.S. Army Waterways Experiment Station, Corps of Engineers, Vicksburg, MS*. 1992.
- Haley, P., M. Jurkat, and P.J. Brady, *NATO Reference Mobility Model, Edition I, Users Guide*, in *Technical Report Number 12503, U.S. Army Tank-automotive and Armaments Command, Warren, MI*. 1979.
- Lunne, T., P.K. Robertson, and J.J.M. Powell, *Cone Penetration Testing in Geotechnical Practice*. 1997, New York: Blackie Academic/Routledge Publishing.
- Jody D. Priddy and W.E. Willoughby, *Clarification of vehicle cone index with reference to mean maximum pressure*. *Journal of Terramechanics*, 2006. **43**(2): p. 85–96.
- Bekker, M.G., *Theory of land locomotion*. 1956: Ann Arbor, MI: University of Michigan Press.
- Bekker, M.G., *Introduction to terrain-vehicle systems*. 1969: Ann Arbor, MI: University of Michigan Press.
- Wong, J.Y., *The theory of ground vehicles*. 4th edition ed. 2008: Wiley.
- Standard Test Method for Shear Testing of Bulk Solids Using the Jenike Shear Cell*. 2007, ASTM International: West Conshohocken, PA.
- Gibbesch, A. and B. Schafer, *Multibody system modelling and simulation of planetary rover mobility on soft terrain*, in *Proc. of the 8th International Symposium on Artificial Intelligence, Robotics and Automation in Space - iSAIRAS'*. 2005: Munich, Germany.
- Krenn, R. and A. Gibbesch, *Soft soil contact modeling technique for multi-body system simulation*. *Trends in Computational Contact Mechanics, Lecture Notes in Applied and Computational Mechanics*, 2011. **58**: p. 135-155.
- Krenn, R. and G. Hirzinger, *SCM – A soil contact model for multi-body system simulation*, in *11th European Regional Conference of the International Society for Terrain-Vehicle Systems*. 2009: Bremen.
- Madsen, J., A. Seidl, and D. Negrut, *Off-Road Vehicle Dynamics Mobility Simulation with a Compaction based deformable terrain model*, in *Proceedings of the ASME 2013 International Design Engineering Technical Conferences & Computers and Information in Engineering Conference*. 2013: Portland, Oregon.
- Madsen, J., et al., *A Physics-Based Vehicle/Terrain Interaction Model for Soft Soil Off-Road Vehicle Simulations*, in *2012 SAE Congress and Exposition*. 2012 SAE: Detroit, MI.
- Pan, W., Y.E. Papelis, and Y. He, *A vehicle-terrain system modeling and simulation approach to mobility analysis of vehicles on soft terrain*, in *Proc. SPIE 5422, Unmanned Ground Vehicle Technology VI, 520*. 2004: Orlando, FL.
- Rubinstein, D. and R. Hitron, *A detailed multi-body model for dynamic simulation of off-road tracked vehicles*. *Journal of Terramechanics*, 2004. **41**: p. 163-173.
- Janosi, Z. and B. Hanamoto, *Analytical determination of drawbar pull as a function of slip for tracked vehicles in deformable soils*, in *1st International Conference on Terrain-Vehicle Systems*. 1961: Turin, Italy.
- SIMPACK, <http://www.simpack.com>. 2014.
- Shoop, S.A., *Finite Element Modeling of Tire-Terrain Interaction*. 2001, US Army Corps of Engineers, Engineer Research and Development Center, Cold Regions Research and Engineering Laboratory: Hanover, NH.
- Shoop, S.A., P.W. Richmond, and J. Lacombe, *Overview of cold regions mobility modeling at CRREL*. *Journal of Terramechanics*, 2006. **43**(1): p. 1-26.
- Grujicic, M., et al., *Finite Element Analysis of the Effect of Up-Armouring on the Off-Road Braking and Sharp-Turn Performance of a High-Mobility Multi-Purpose Wheeled Vehicle*. *Proceedings of the Institution of Mechanical Engineers, Part D: Journal of Automobile Engineering*, 2009. **223**(11): p. 1419-1434.
- Xia, K.M., *Finite element modeling of tire/terrain interaction: Application to predicting soil compaction and tire mobility*. *Journal of Terramechanics*, 2011. **48**(2): p. 113-123.
- Li, H., *Analysis of off-road tire-soil interaction through analytical and finite element methods*, in *Department of Mechanical Engineering*. 2013, University of Kaiserslautern: Germany.
- Ragheb, H., M. El-Gindy, and H.A. Kishawy, *Multi-Wheeled Combat Vehicle Modeling on Rigid and Soft Terrain*, in *2013 NDIA Ground Vehicle Systems Engineering and Technology Symposium, Modeling & Simulation, Testing and Validation (MSTV) mini-symposium*. 2013: Troy, MI.

Prediction of Vehicle Mobility on Large-Scale Soft-Soil Terrain Maps Using Physics-Based Simulation, Wasfy, et al.
UNCLASSIFIED: Distribution Statement A. Approved for public release; distribution is unlimited. #27972

24. Jafari, H., *3D finite element model to simulate the rolling resistance of a radial ply tire vali-dated by experiments in soil bin testing facility*. Journal of Advances in Vehicle Engineering, 2015. **1**(2): p. 37-45.
25. Wright, A., *Tyre / Soil Interaction Modelling withing a Virtual Proving Ground Environment*, in *School of Applied Sciences*. 2012, Cranfield University.
26. Ti, K.S., et al., *A Review of Basic Soil Constitutive Models for Geotechnical Application*. Electronic Journal of Geotechnical Engineering, 2009. **14**: p. 1-18.
27. Drucker, D.C. and W. Prager, *Soil mechanics and plastic analysis for limit design*. Quarterly of Applied Mathematics, 1952. **10**(2): p. 157 - 165.
28. Sandler, I.S. and D. Rubin, *An Algorithm and a Modular Subroutine for the Cap Model*. International Journal for Numerical and Analytical Methods in Geomechanics, 1979. **3**: p. 173-186.
29. *Abaqus, Simulia*. [cited 2016; Available from: <http://www.3ds.com/products-services/simulia/products/abaqus/>].
30. *PAM-CRASH*. [cited 2016; Available from: <http://www.esi-group.com>].
31. *LS-DYNA*. [cited 2016; Available from: <http://www.lstc.com/products/ls-dyna>].
32. Cundall, P.A. and O.D.L. Strack, *A discrete numerical model for granular assemblies*. Geotechnique, 1979. **29**(1): p. 47-65.
33. Cundall, P.A., *A computer model for simulating progressive large-scale movements in block rock mechanics*, in *Proc. Symp. Int. Soc. Rock Mech*. 1971: Nancy.
34. Carrillo, A., et al., *Design of a Large Scale Discrete Element Soil Model for High Performance Computing Systems*, in *Proceeding of the Supercomputing '96 Proceedings of the 1996 ACM/IEEE conference on Supercomputing*. 1996, ACM.
35. Horner, D., J. Peters, and A. Carrillo, *Large Scale Discrete Element Modeling of Vehicle-Soil Interaction*. Journal of Engineering Mechanics, 2001. **127**: p. 1027-1032.
36. Peters, J.F., et al., *A poly-ellipsoid particle for non-spherical discrete element method*. Engineering Computations, 2009. **26**(6).
37. Nakashima, H. and A. Oida, *Algorithm and implementation of soil-tire contact analysis code based on dynamic FE-DE method*. Journal of Terramechanics, 2004. **41**(2/3): p. 127-137.
38. Smith, W. and H. Peng, *Modeling of wheel-soil interaction over rough terrain using the discrete element method*. Journal of Terramechanics, 2013. **50**(5-6): p. 277-287.
39. Negrut, D., et al., *Investigating the mobility of light autonomous tracked vehicles using a high performance computing simulation capability*, in *2012 NDIA Ground Vehicle Systems Engineering and Technology Symposium, MSTV Mini-symposium*. 2012: Troy, MI.
40. Negrut, D., et al., *Investigating Through Simulation the Mobility of Light Tracked Vehicles Operating on Discrete Granular Terrain*, in *SAE World Congress*. 2013, SAE: Detroit, MI.
41. Tasora, A., et al., *A Compliant Visco-Plastic Particle Contact Model Based on Differential Variational Inequalities*. International Journal of Non-Linear Mechanics, 2013.
42. Wasfy, T.M., H.M. Wasfy, and J.M. Peters, *Coupled Multibody Dynamics and Discrete Element Modeling of Vehicle Mobility on Cohesive Granular Terrains*, in *10th International Conference on Multibody Systems, Nonlinear Dynamics, and Control (MSNDC), ASME 2014 International Design Engineering Technical Conferences*. 2014: Buffalo, NY.
43. Wasfy, T.M., H.M. Wasfy, and J.M. Peters, *High-Fidelity Multibody Dynamics Vehicle Model Coupled with a Cohesive Soil Discrete Element Model for predicting Vehicle Mobility*, in *11th ASME International Conference on Multibody Systems, Nonlinear Dynamics, and Control (MSNDC)*. 2015: Boston, MA.
44. *DIS (Dynamic Interactions Simulator)*. 2016 [cited 2016; Available from: <http://www.ascience.com/ScProducts.htm>].
45. Monaghan, J., *Smoothed Particle Hydrodynamics*. Rep. Prog. Phys., 2005. **68**: p. 1703–1759.
46. Monaghan, J. and R.J. Gingold, *Smoothed Particle Hydrodynamics*. Mon. Not. Roy. Astr. Soc., 1977. **181**: p. 375-389.
47. Lescoe, R., et al., *Tire-Soil Modeling Using Finite Element Analysis and Smooth Particle Hydrodynamics Techniques*, in *2010 ASME International Design Engineering Technical Conferences and Computers and Information in Engineering Conference*. 2010.
48. Dhillon, R., et al., *Development of Truck Tire-Soil Interaction Model using FEA and SPH*, in *Proceedings of SAE 2013 World Congress*. 2013, SAE: Detroit, MI.
49. Sulsky, D., S.-J. Zhou, and H. Schreyer, *Application of particle-in-cell method to solid mechanics*. Comp. Phys. Comm., 1995. **87**: p. 236–252.
50. Stomakhin, A., et al., *A material point method for snow simulation*. ACM Transactions on Graphics, 2013. **32**(4): p. Article 102.
51. Al-Kafaji, I.K.J., *Formulation of a Dynamic Material Point Method (MPM) for Geomechanical Problems*. 2013, Universität Stuttgart.
52. Wasfy, T.M., *Lumped-parameters brick element for modeling shell flexible multibody systems*, in *18th Biennial Conference on Mechanical Vibration and Noise*. 2001, ASME International Pittsburgh, PA.

53. Wasfy, T.M., *Edge projected planar rectangular element for modeling flexible multibody systems*, in *19th Biennial Conference on Mechanical Vibration and Noise*. 2003, ASME International: Chicago, IL.
54. Wasfy, T.M., Noor, A.K., *Modeling and sensitivity analysis of multibody systems using new solid, shell and beam elements*. *Computer Methods in Applied Mechanics and Engineering*, 1996. **138**(1-4): p. 187-211.
55. Wasfy, T.M., *A torsional spring-like beam element for the dynamic analysis of flexible multibody systems*. *International Journal for Numerical Methods in Engineering*, 1996. **39**(7): p. 1079-1096.
56. Wasfy, T.M., *Modeling spatial rigid multibody systems using an explicit-time integration finite element solver and a penalty formulation*, in *Proceeding of the DETC: 28th Biennial Mechanisms and Robotics Conference*. 2004, ASME International: Salt Lake, Utah.
57. Leamy, M.J., Wasfy, T.M., *Transient and steady-state dynamic finite element modeling of belt-drives*. *ASME Journal of Dynamics Systems, Measurement, and Control*, 2002. **124**(4): p. 575-581.
58. Wasfy, T.M., *Asperity spring friction model with application to belt-drives*, in *19th Biennial Conference on Mechanical Vibration and Noise*. 2003, ASME International: Chicago, IL.
59. Wasfy, T.M., Wasfy, H.M, and Peters, J.M., *Real-time explicit flexible multibody dynamics solver with application to virtual-reality based e-learning*, in *Proceedings of the ASME 2011 International Design Engineering Technical Conferences & Computers and Information in Engineering Conference (IDETC/CIE 2011), 8th International Conference on Multibody Systems, Nonlinear Dynamics, and Control*. 2011, ASME: Washington, DC.
60. Wasfy, T.M., O’Kins, J. and Ryan, D., *Experimental validation of a multibody dynamics model of the suspension system of a tracked vehicle*, in *2011 NDIA Ground Vehicle Systems Engineering and Technology Symposium*. 2011, NDIA: Dearborn, MI.